Research Article

Microstructural characterization and dielectric properties of single crystalline $BaTi_2O_5$ nanowires prepared by molten-salt method

Xianzhuo Wang[1] · Kai Leng[1] · Zhipeng Pei[1] · Weiren Xia[1] · Heng Wu[1] · Yao Lu[1] · Xinhua Zhu[1]

Abstract

$BaTi_2O_5$ (BT2) nanowires were successfully prepared via molten-salt method. The effects of synthesized temperature, dwell time, and molten salt concentration on the formation of BT2 nanowires were studied. X-ray diffraction patterns reveal that the BT2 nanowires crystallize in a monoclinic crystal structure. Neither the longer dwell time nor molten salt concentration has apparent influence on the formation of BT2 phase structure, whereas the synthesized temperature exerts great effect on the morphology of BT2 nanowires. One-dimensional morphology of the BT2 products was only obtained at a narrow temperature window (870–900 °C). At 970 °C, the morphology of BT2 nanowires was destroyed and they are broken into particles, growing as large flat crystals. The BT2 nanowires synthesized at 900 °C exhibit uniform morphology and grow in the [010] direction, which have an average diameter of 780 nm and length of 15 μm. The formation mechanism of BT2 nanowires in the MSS process is proposed. The BT2 nanowires exhibit the single-crystalline characteristics, as proven by high-resolution TEM images and electron diffraction patterns. Quantitative X-ray energy-dispersive spectroscopy analysis shows the BT2 nanowires having homogeneous chemical compositions, and their atomic cation ratio of Ba:Ti is 1:2.16. Dielectric properties of the BT2 nanowires synthesized at 900 °C are measured at room temperature with the frequency ranged from 10^2 to 10^6 Hz. The BT2 nanowires exhibit almost frequency independent dielectric behavior with dielectric constants of 28–31. The dielectric losses remain constant value of ~ 0.02 below 10^5 Hz, and increase up to 0.04 at 10^6 Hz.

Keywords Molten salt synthesis (MSS) · $BaTi_2O_5$ nanowires · Dielectric properties · Raman spectra · Microstructure characterization

1 Introduction

The ferroelectricity in $BaTi_2O_5$ (BT2) compound was discovered in 2003, and since then much attention has been given to this compound [1–8]. For example, Akashi et al. reported the high dielectric constant (in the range 20,000–30,000) in BT2 single crystal along the [010] direction and high Curie temperature of 460 °C, and much small dielectric loss [1, 2]. To obtain the basic knowledge of the BT2 crystal structure and the mechanism of its phase transition, different structural analysis techniques (e.g., synchrotron x-ray diffraction, micro-Brillouin and Raman scattering, and neutron powder diffraction) have been used by some researchers [4, 7, 9]. Their results demonstrate that the BT2 crystallizes in a monoclinic phase structure, which is homogeneous (unlike that of $BaTiO_3$) and in one of three TiO_6 octahedral units, Ti shifts along the *b* axis opposite from the oxygen in the TiO_6 octahedral unit, leading to the ferroelectricity. The phase transition of BT2 from paraelectric *C*2/m to ferroelectric *C*2 can be categorized as displacive type with large damping of the soft A_u mode [9]. Meanwhile, the piezoelectric response of BT2 compound is also investigated by first-principles calculations [6]. It is found that the piezoelectric constant e_{22} (= 2.02 C/m^2) for BT2 crystal is comparable to that of $PbTiO_3$ (the calculated e_{33} = 3.3 C/m^2). Therefore, BT2 is a promising materials used

✉ Xinhua Zhu, xhzhu@nju.edu.cn | [1]National Laboratory of Solid State Microstructures, School of Physics, Nanjing University, Nanjing 210093, China.

SN Applied Sciences (2019) 1:528 | https://doi.org/10.1007/s42452-019-0553-x

Received: 21 March 2019 / Accepted: 2 May 2019 / Published online: 6 May 2019

as lead-free piezoelectrics. With the rapid development of microelectronics technology, the feature sizes of microelectronic devices based on ferroelectric oxide materials are becoming smaller, entering into the nanometer-sized scale. Today, the lateral size of the smallest solid-state Flash memory cell is only ~ 80 nm [10], and it will be continuously decreased in the near future. Due to the size effects low-dimensional ferroelectric oxide nanostructures exhibit much novel physical and chemical properties as compared with their bulk and film counterparts. Therefore, ferroelectric oxide nanowires have attracted extensive interest for potential applications in the nanosacle memories, sensors, actuators, and energy harvesters [11–13]. As a new ferroelectric oxide, the synthesis and characterization of BT2 1D (one-dimensional) nanostructures are becoming much important due to its promising applications in the next generation oxide nanoelectronic devices.

Up to date, various techniques (e.g., solid-state reaction method, spark plasma sintering, arc melting, sol–gel method, hydrothermal reaction, and pulsed laser deposition) have been used to synthesize BT2 samples in the forms of single crystals [1, 2, 5], ceramics [14–19], fine powders [20, 21], and thin films [22–25]. However, up to date only a few works reporting on BT2 1D nanostructure are available [26–29]. For example, BT2 nanobelts were synthesized by Wang et al. via the hydrothermal synthesis in two-step process [26]. The width of nanobelts was measured to be about 200–300 nm, and their thickness varied from 60 to 100 nm. Their length was up to several micrometers. Single-crystalline BT2 nanobelts with widths in the range of 30–500 nm and the length up to several hundred micrometers, were also synthesized via molten salt synthesis (MSS) route [27], where the $BaTiO_3$ polycrystal powders were used as the precursors and the eutectic NaCl–KCl chlorides were used as molten-salt medium. Beside the single-crystalline BT2 nanobelts, single-crystalline BT2 nanowires were also prepared by MSS method [28], where $BaC_2O_4{\cdot}H_2O$ and TiO_2 were selected as the starting materials. The BT2 nanowires had a length over tens of micrometers and their cross-section exhibited a rectangular morphology with width of 80–200 nm and thickness of 70–150 nm. An intermediate phase of $Ba_4Ti_{13}O_{30}$ with 1D morphology was formed during MSS process, which was believed to facilitate the formation of BT2 nanowires. However, the exact transferring process from the intermediate phase of $Ba_4Ti_{13}O_{30}$ to BT2 was not investigated. Local piezoresponse force microscopy images revealed a switchable polarization of the BT2 nanowires at room temperature, and the highest value of effective d_{33} was reported to be ~ 300 pm/V [28]. In addition to the nanobelts and nanowires, BT2 nanopillars with (010)-orientation were also reported [29]. The nanopillars had a width of about 250–400 nm and length of 2.5 μm. Recently, BT2 nanowires are also used as templates for the synthesis of perovskite oxide nanorods such as $BaTiO_3$ [30, 31] and $(Ba,Sr)TiO_3$ [32].

Despite of the previous research activities performed on BT2 1D nanostructures such as nanowires, nanobelts, and nanopillars, there are still be lacking in the dielectric data and atomic-scale microstructural analyses of BT2 1D nanowires. In addition, the growth mechanism of the BT2 nanowires during the MSS process is not well understood. Basically, in the process of MSS method, there exists two fundamental reaction mechanisms during the formation of the final products [33]. The first one is all the reactant oxides are fully dissolved within the molten salt and they diffuse to react in a short time. One representative model is the Bi_2WO_6 system [34], where the Bi_2WO_6 particles are formed via complete dissolution of the constituent oxides (e.g., WO_3 and Bi_2O_3) in the KCl–NaCl eutectic mixed salts at 650 °C for 1 h and the complete reactions between WO_3 and Bi_2O_3 starting materials. The second one is that among the starting materials some reactants are much more soluble within the molten salt than the other components, therefore, they easily diffuse onto the surfaces of the other less soluble components and react with them, forming the final products with a similar morphology as the less soluble reactants. A typical example is template-free fabrication of pure single-crystalline perovskite oxide nanorods/nanowires by MSS method at relatively high temperature and large ratios of the salt to the precursors [35, 36]. In the normal MSS procedure [37–39], the starting oxide materials are mixed with selected molten salts and heated to the desired temperatures. However, this procedure usually facilitates the perovskite oxide formation process starting before the system reaching the desired temperature, even before the salt melting. That hinders the investigations on the influence of temperature and other factors on the formation of the final products. Recently, Vradman et al. [40] proposed a modified MSS procedure named as "feeding" procedure, where the starting precursors were fed into the molten salt with the desired temperature rather than they were mixed together and heated in a alumina crucible. The main feature of the "feeding" procedure is the starting perovskite formation temperature, which is clear-cut in "feeding" procedure, just starting at desired temperature. In the 'feeding" procedure, the nucleation rate is more significant, resulting in the formation of smaller crystals, whereas in the normal MSS procedure (starting precursors mixed and heated together with the molten salts) perovskite formation process begins at a significantly lower temperature where the crystal growth is more dominant than nucleation, leading to much larger particles. These results expound the formation mechanistic aspects of the perovskite oxides in molten salts involving nucleation and crystal growth phenomena.

In the present work, single-crystalline BT2 nanowires were synthesized via MSS route. The influence of synthesized temperature, dwell time, and molten salt concentration on the growth of BT2 nanowires are investigated. Microstructures of the BT2 nanowires were also characterized at atomic-scale by high-resolution TEM. In addition, the Raman spectroscopy is utilized to probe lattice dynamics and to examine the phase structure of the BT nanowires. Growth mechanism of the BT2 nanowires during the MSS process is proposed and their growth along the [010] direction is also discussed from the crystal structure of BT2. Dielectric properties of the BT2 nanowires are also measured at room temperature under different frequencies. The results demonstrate that the BT2 nanowires exhibit almost frequency-independent dielectric behavior with dielectric constants of 28–31. The corresponding dielectric losses remain nearly constant of ~ 0.02 below 10^5 Hz, and increase up to 0.04 at 10^6 Hz. The present dielectric data promote the BT2 nanowires to be more attractive for nanoscale dielectric devices.

2 Experimental procedures

2.1 Synthesis of BT2 nanowires via MSS route

BT2 nanowires were synthesized via MSS route, where analytical grade BaC_2O_4, TiO_2, and the NaCl–KCl eutectic mixed salts were mixed together with the molar ratios of BaC_2O_4:TiO_2:NaCl:KCl equal to 1:2:20:20, 1:2:30:30, and 1:2:40:40, respectively. The mixture was ground for 30 min, and then transferred into alumina crucible and calcined at 770–970 °C for 6–9 h. Subsequently, the samples were cooled in a furnace naturally to room temperature. After calcination, the samples were thoroughly washed with deionized water several times until no free Cl^- ions were detected by $AgNO_3$ solution, to ensure the molten chloride salts were complete removed. Finally, the samples were dried in an oven at 120 °C for 4 h.

2.2 Microstructural characterization of BT2 nanowires

Powder X-ray diffraction (XRD) was utilized to characterize the crystal structure of BT2 nanowires, which was performed on a X-ray diffractometer (Rigaku D/Max-RA) with CuKα radiation (λ = 0.15406 nm). The morphology of the as-prepared BT2 nanowires were revealed by scanning electron microscopy (SEM, Hitachi S-3100H, Japan) equipped with energy-dispersive X-ray spectra (EDS) to carry out compositional analysis. High-resolution transmission electron microscopy (HR-TEM) images and electron diffraction patterns were recorded on Tecnai G2 (S-Twin) microscope operated at 200 kV. The specimens used for HR-TEM observations were prepared as followings. First, the as-prepared BT2 nanowires were ultrasonically dispersed in ethanol for 20 min to disperse the nanowires well in ethanol. And then a small drop of suspension was placed on carbon-coated grids by using pipette and wait it for drying naturally. Raman spectra of the as-prepared BT2 nanowires were recorded at room temperature by a Raman spectrophotometer (Model 2501 PC, Shimadzu) with the wavelength in the range of 300–600 nm, employing an Ar^+ laser for excitation (λ = 514 nm).

2.3 Dielectric properties of BT2 nanowires

Before dielectric measurements, small disks (10 mm in diameter and 2 mm in thickness) were obtained from the BT2 nanowires (synthesized at 900 °C for 9 h by MSS method) under 8 MPa pressure, and then they were post-synthesized at 800 °C for 2 h in air. After polishing, silver paste was pained on the annealed disks and fired at 550 °C for 30 min as electrodes. The dielectric properties of the BT2 nanowires were evaluated by an Agilent 4192A impedance-analyzer at room temperature and the frequency from 10^2 to 10^6 Hz.

3 Results and discussion

3.1 XRD analysis of BT2 nanowires

Figure 1 demonstrates the XRD patterns of three BT2 samples synthesized at 870 °C for 9 h under different molar ratios of BaC_2O_4:TiO_2:NaCl:KCl. It is observed that all the XRD peaks are well in agreement with that of the monoclinic crystalline BT2 crystal structure (JCPDS

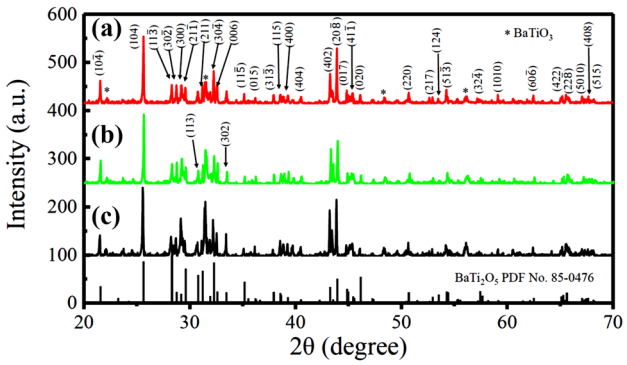

Fig. 1 XRD patterns of the $BaTi_2O_5$ products synthesized at 870 °C for 9 h under the molar ratios of BaC_2O_4:TiO_2:NaCl:KCl equal to (a) 1:2:20:20, (b) 1:2:30:30, and (c) 1:1:40:40, respectively. The standard XRD pattern from the $BaTi_2O_5$ (JCPDS No. 85-0476) is also presented for comparison

card No. 85-0476, unit-cell parameters $a = 0.9410$ nm, $b = 0.3930$ nm, $c = 1.6892$ nm, and $\alpha = \gamma = 90°$, $\beta = 103.03°$), except several minor impurity peaks attributed from the $BaTiO_3$ phase (JCPDS No. 031-0174) and marked with stars in Fig. 1. That indicates the formation of almost pure phase of BT2. The unit cell parameters (a, b, c, and β) of the monoclinic BT2 nanowires can be calculated by the following equation:

$$\frac{1}{d_{hkl}^2} = \frac{1}{\sin\beta^2}\left(\frac{h^2}{a^2} + \frac{l^2}{c^2} - \frac{2hl}{ac}\cos\beta\right) + \frac{k^2}{b^2} \quad (1)$$

where d_{hkl} is the interplanar spacing between the neighboring (hkl) planes, a, b and c are the magnitude of the lattice vectors $\vec{a}$, $\vec{b}$, and $\vec{c}$, respectively, and β is the angle between the lattice vectors $\vec{a}$ and $\vec{c}$. Based on the XRD patterns shown in Fig. 1, the lattice parameters (a, b, and c) of the monoclinic BT2 nanowires can be determined to be $a = 0.9356$ nm, $b = 0.3947$ nm, and $c = 1.6914$ nm, and $\beta = 103.0°$, which are slightly modified as compared with the data of JCPDS card No. 85-0476. From the corresponding three XRD patterns (Fig. 1) it is found that the formation of BT2 phase structure is almost not influenced by the molar ratio of BaC_2O_4:TiO_2:NaCl:KCl. That implies different amount of the NaCl–KCl eutectic salts acts only as a reaction medium in the MSS procedure, providing a melt environment to accelerate the MSS reaction. Figure 2 displays the XRD patterns of two BT2 samples, which were synthesized by MSS method at 870 °C with dwell time of 6 h and 9 h, respectively. It is found that the two BT2 samples exhibit almost the same XRD patterns. That means under the longer dwell time the formation of BT2 phase structure is completed. To reveal the phase structure evolution, a series of studies of the samples with different reaction times are needed. In the previous work, Leng et al. [41] reported on the effect of dwell time on the phase structure evolution of the BT2 powders synthesized at 840 °C by MSS method, where analytical grade $BaCO_3$ and TiO_2 were used as precursors, and the NaCl–KCl eutectic mixed salt was used as molten salt. The XRD patterns revealed that the synthesized powders were mainly composed of $BaCO_3$, $BaTiO_3$, BT2, and small amount of TiO_2 as the dwell time was 0.5 h, whereas when the dwell time was over 1.50 h, the impure phase of $BaCO_3$ was reduced gradually but the BT2 phase content was increased. Finally, when the dwell time was increased up to 5 h, the synthesized powders had a pure phase structure of BT2. Therefore, in the present work, the samples synthesized at 870 °C by MSS method with dwell times of 6 h and 9 h had almost the same XRD patterns because the formation of BT2 phase structure was already completed. To understand the role of synthesized temperature, five BT2 samples were also synthesized at different temperatures but the same dwell time (9 h). The corresponding XRD results are shown in Fig. 3, where all the XRD peaks can be readily indexed to the monoclinic BT2 crystal structure (JCPDS card No. 85-0476), and no impure phase is observed. While the synthesized temperature was increased up to 870 °C (Fig. 3c) or 900 °C (Fig. 3d), their XRD patterns are very similar, and all the XRD diffraction peaks are well in agreement with the JCPDS card 85-0476. That implies the synthesized BT2 samples at 870 °C or 900 °C were pure phase structure of BT2. However, the samples synthesized at 930 °C exhibit very different XRD pattern, as shown in Fig. 3d. It was observed that the intensity of the (311) diffraction became much strong, its intensity was even higher than the (104) main diffraction peak, indicating the preferred orientation growth in the BT2 product synthesized at 930 °C. In the XRD pattern of the BT2 product synthesized at 970 °C (Fig. 3e), only two strong XRD diffraction peaks contributed from (113) and (311) planes were observed, whereas the (104) main XRD diffraction peak was almost completely depressed. That indicated

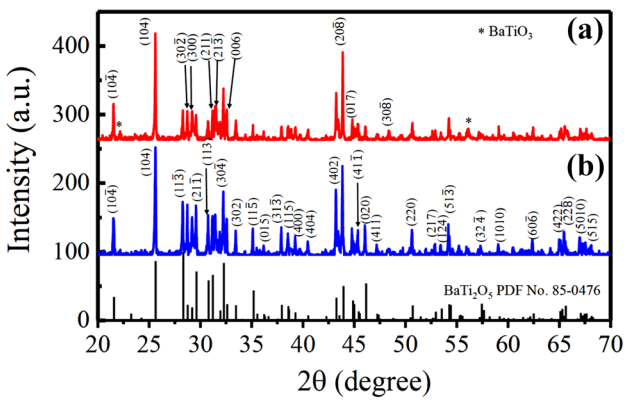

Fig. 2 XRD patterns of the $BaTi_2O_5$ products synthesized at 870 °C for dwell time of (a) 6 h and (b) 9 h under the molar ratio of BaC_2O_4:TiO_2:NaCl:KCl equal to 1:2:20:20. The standard XRD pattern from $BaTi_2O_5$ (JCPDS No. 85-0476) is also presented for comparison

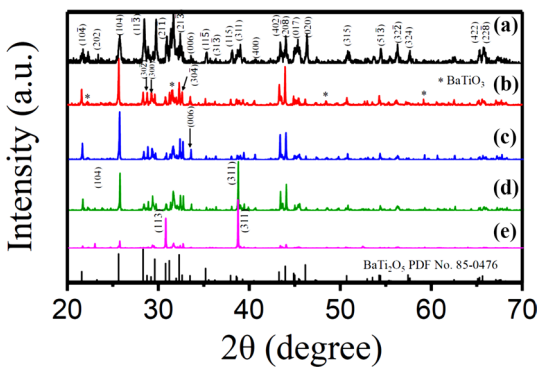

Fig. 3 XRD patterns of the $BaTi_2O_5$ products synthesized at (a) 770 °C, (b) 870 °C, (c) 900 °C, (d) 930 °C, and (e) 970 °C for 9 h under the molar ratio of BaC_2O_4:TiO_2:NaCl:KCl equal to 1:2:20:20

a bimodal of the preferred orientation growth appeared in this BT2 sample synthesized at 970 °C. Actually, the corresponding SEM image (see below) reveal that many plate-like BT2 particles with the (113) or (311) preferred orientation are formed in the BT2 sample synthesized at 970 °C. Therefore, the synthesized temperature plays an important impact on the preferred orientation growth of the BT2 samples. In contrast, neither molten salt content nor dwell time exerts substantial effect on the preferred orientation growth and phase structure of the BT2 products synthesized by MSS method.

3.2 Microstructural characterizations of BT2 products

SEM images of the synthesized BT2 samples at temperature ranged from 870 to 970 °C, are shown in Fig. 4. Figure 4a demonstrates the SEM image of the BT2 products synthesized at 870 °C, and Fig. 4a-1, a-2 shows the corresponding histograms of the length and diameter of the BT2 products. It is found that the BT2 products exhibit 1D morphology of nanowires, their lengths in range of 3.0–34.0 μm (Fig. 4a-1) and diameters with a wide distribution in a range of 270 nm–3.0 μm (Fig. 4a-2). Their average diameter was determined to be ~ 900 nm and the average length was about 13.0 μm. The morphology of the as-synthesized BT2 nanowires synthesized at 900 °C are shown in Fig. 4b, and b-1, b-2 illustrates the corresponding histograms of the length and diameter of the BT2 nanowires. It is observed that the BT2 nanowires have a uniform morphology. Their average diameter is 800 nm and the average length is 15.0 μm. As the synthesized temperature was increased up to 930 °C (Fig. 4c), the average diameter of the BT2 nanowires was increased up to ~ 1.10 μm whereas the average length was reduced to ~ 14.0 μm. That was due to that the morphology of BT2 nanowires was broken and they were decomposed into particles. Further increasing the synthesized temperature to 970 °C, many BT2 nanowires were broken and they are decomposed into particles, which grew into large flat crystals as large as 20 μm (width) × 35 μm (length) (see Fig. 4d). The volume fraction of the BT2 nanowires in the final product was reduced to 70%. The statistic distributions of the length and diameter of the BT2 nanowires are shown in Figs. 4d-1, d-2. The average diameter and length of the BT2 nanowires are ~ 1.50 μm and 13.0 μm, respectively. The above SEM images show that the uniform morphology of the BT2 nanowires can be only obtained in a limited synthesized temperature window. That is due to that the crystal structure of BT2 contains many different linkage modes of the $[TiO_n]$ polyhedron, especially the edge-sharing mode, resulting in a metastable monoclinic BT2 structure rather than a stable one [42]. EDS measurements can provide the chemical information of the BT2 nanowires. A typical EDS spectrum acquired from the BT2 nanowires synthesized at 900 °C in a mapping mode rather than the punctual dot mode is shown in Fig. 5, which shows that the BT2 nanowires are composed of Ba, Ti, and O elements, and the Ba: Ti (atomic ratio) is about 1:2.16 (see inset), close to the nominal value. Besides the Ba, Ti, and O elements, other elements such as Na, K, Cl are not detected in the present EDS spectrum, indicating the samples are completely free from the NaCl–KCl molten salts by washing with deionized water. The signal of carbon is from the carbon conductive band used for preparation of the SEM samples. The quantitative EDS analyses for the BT2 nanowires synthesized at other temperatures also demonstrate that the measured Ba:Ti atomic ratios were about 1: 2.16, indicating the cation atomic ratios of Ba:Ti in the BT2 nanowires close to the nominal value.

TEM can provide further insights into the microstructures of the as-synthesized BT2 nanowires. Figure 6a shows the TEM image of the BT2 nanowires synthesized at 900 °C for 9 h, where several individual BT2 nanowires are observed. The average diameter of the BT2 nanowires was measured to be 260 nm. An enlarged TEM image of the top-end of one BT2 nanowire is shown Fig. 6b, c displays the SAED pattern recorded from the BT2 nanowire, which has the characteristics of single-crystal diffraction pattern and can be indexed to the reflection from a monoclinic BT2 crystal along the [100] zone axis. Therefore, the SAED pattern proves the single-crystallinity of the BT2 nanowires. Figure 6d displays the HRTEM image taken from the top-end of the BT2 nanowire along the [100] direction, where the lattice fringes in the *b*–*c* plane are observed. The distance between the lattice fringes observed in the [001] direction was measured to be 8.42 Å, close to the (002) plane spacing (8.45 Å) of the BT2 structure. The corresponding Fourier-filtered HRTEM image is shown in Fig. 6e, where the lattice fringes along [001] and [010] directions are clearly observed, indicating the BT2 nanowires growing in the [010] direction. The growth of BT2 nanowire along the *b*-axis can be understood from the crystal structure of the monoclinic BT2. As reported by Yashima et al. [7], in an unit cell of ferroelectric BT2 crystal structure with noncentro-symmetric *C*2 space group, there are three kinds of Ti sites (e.g., Ti1, Ti2, and Ti3) and two kinds of Ba sites (e.g., Ba1 and Ba2). Figure 7a schematically shows the connections between the $[TijO_6]$ octahedra (site position $j = 1$, 2, and 3) in the *a*–*c* plane, and in the *b*–*c* plane as illustrated in Fig. 7b. It is noticed that in the *a*–*c* plane a $[Ti_1O_6]$ octahedron is linked with $[Ti_2O_6]$ octahedron by edge-sharing, but with $[Ti_3O_6]$ and $[Ti_1O_6]$ octahedra by corner-sharing. In the *b*-*c* plane, the $[Ti_2O_6]$ and $[Ti_3O_6]$ octahedra are linked through edge-sharing, but the $[Ti_2O_6]$ octahedron is linked with $[Ti_1O_6]$ octahedron via

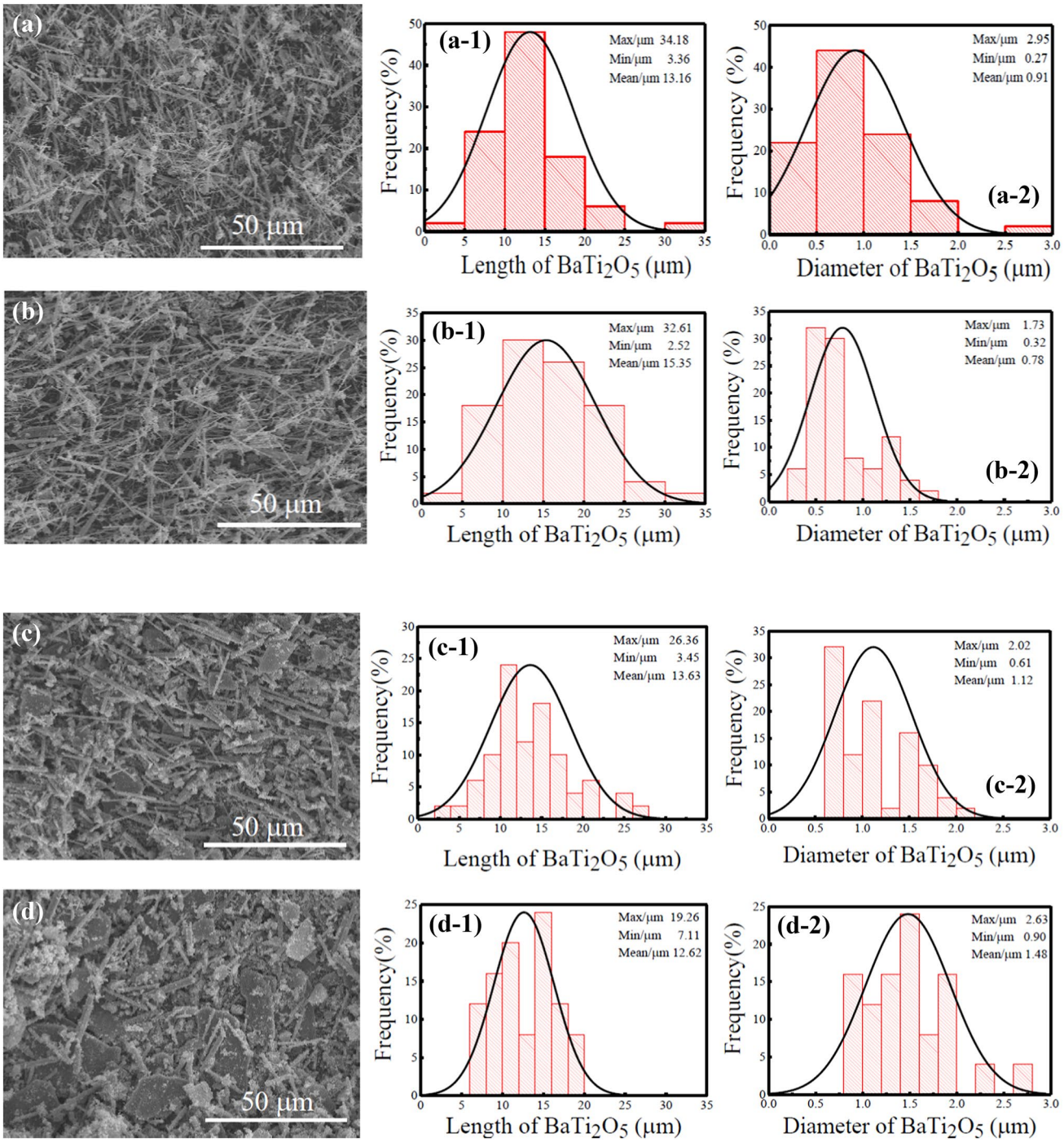

Fig. 4 SEM images of the $BaTi_2O_5$ nanowires synthesized at **a** 870 °C, **b** 900 °C, **c** 930 °C, and **d** 970 °C for 9 h under the molar ratio of BaC_2O_4:TiO_2:NaCl:KCl equal to 1:2:20:20, and the corresponding histograms of the length and diameter distributions of the BT2 nanowires

corner-sharing. One of the three Ti sites (Ti_1) shifts in the opposite direction from the oxygen in the [TiO_6] octahedral unit along the *b* axis (as marked in Fig. 7b), resulting in the ferroelectricity along the [010] direction, whereas the other two Ti sites (Ti_2 and Ti_3) and their corresponding oxygen atoms shift in the same direction [1, 7]. Therefore, the polarization formation in [010] direction can be ascribed to the Ti^{4+} ions' shifting along the *b* axis opposite the displacement of O^{2-} ions within an oxygen octahedral unit at low temperature. During the formation process of BT2 nanowires via the MSS route, BaC_2O_4 first decomposes into α-$BaCO_3$ and CO as the synthesized temperature is

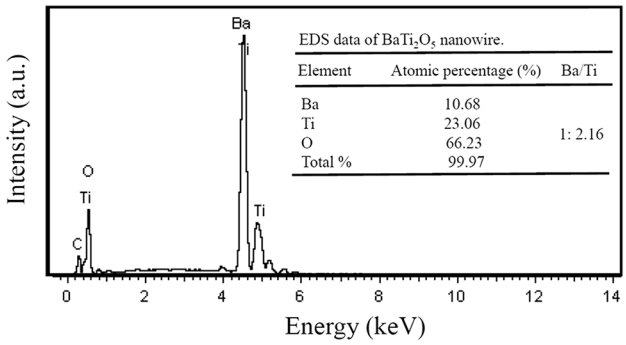

Fig. 5 Typical EDS spectrum obtained from the BT2 nanowires synthesized at 900 °C for 9 h. Inset is the EDS data of the compositions of BT2 nanowires

ranged from 350 to 530 °C, and at 814 °C α-$BaCO_3$ transfers to β-$BaCO_3$, which decomposes into BaO and CO_2 as the temperature is over 840 °C [43]. BaO dissolves into the molten salt liquid and reacts with TiO_2 via the chemical reaction of $BaO + 2TiO_2 \rightarrow BaTi_2O_5$, forming the BT2 nanocrystallites. These BT2 nanocrystallites would prefer to aggregate and self-polarize along the polar *b*-axis, thus, promote the growth of BT2 nanowires in the [010] direction. The formation mechanism of BT2 nanowires in the MSS process is proposed, as schematically shown in Fig. 7c. Furthermore, some small fine nanoparticles adhered to the BT2 nanowires are also observed, as demonstrated in Figs. 6a and 7c, respectively. The EDS spectrum collected from these fine nanoparticles confirms that they are BT2 nanoparticles with the Ba: Ti (atomic ratio) of ~ 1:2.11, close to the nominal value of BT2. This indicates that the BT2 nanowires grow following the Ostwald ripening mechanism [44].

3.3 Raman spectrum of BT2 nanowires

Figure 8 shows a representative room temperature Raman spectrum of the BT2 nanowires, which were synthesized at 900 °C for 9 h with the molar ratio of BaC_2O_4:TiO_2:NaCl:KCl equal to 1:2:20:20. Twenty distinct Raman peaks originating from the phonon modes were clearly observed. The lowest frequency phonon mode was observed at 77 cm^{-1}, and four strongest phonon modes were observed at 218, 280, 342, and 591 cm^{-1}, respectively. Other Raman peaks were observed at 98, 140, 153, 184, 244, 310, 371, 414, 438, 486, 526, 646, 705, 781, and 881 cm^{-1}, respectively. The present Raman peaks of the BT2 nanowires are consistent with those reported for BT2 single crystals [45] and powders [9]. The Raman active modes in BT2 crystals can be predicted by group theoretical analysis based on its space group. It is

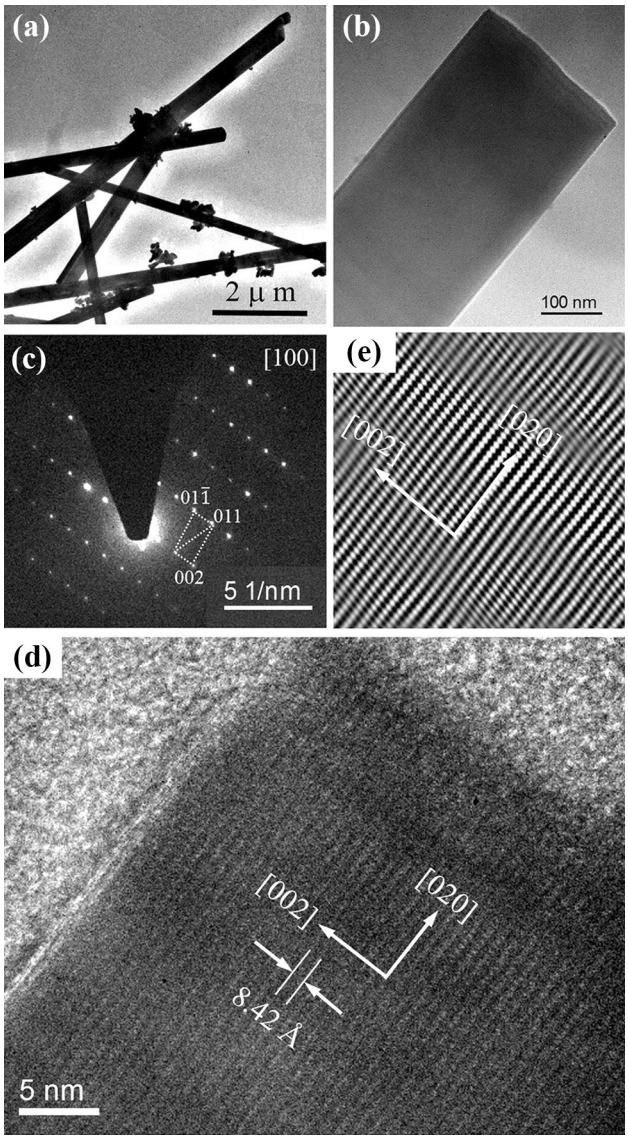

Fig. 6 **a** TEM image of the $BaTi_2O_5$ nanowires synthesized at 900 °C (for 9 h) under the molar ratio of BaC_2O_4:TiO_2:NaCl:KCl equal to 1:2:20:20. **b** TEM image taken from a single $BaTi_2O_5$ nanowire. **c** Selected area electron diffraction (SAED) pattern recorded from the $BaTi_2O_5$ nanowire shown in (**b**). **d** HRTEM image of the top-end of the $BaTi_2O_5$ nanowire, and **e** the corresponding Fourier-filtered HRTEM image

demonstrated that $34A + 35B$ Raman modes are active in the ferroelectric BT2with *C*2 space group, whereas only $12A_g + 24B_g$ Raman modes are active in the paraelectric BT2 with *C*2/m space group [9, 45]. The observed Raman peak numbers in the present BT2 nanowires are less than that predicted by group theory analysis, which is due to the structural distortions of [TiO_6] octahedral units in BT2 nanowires.

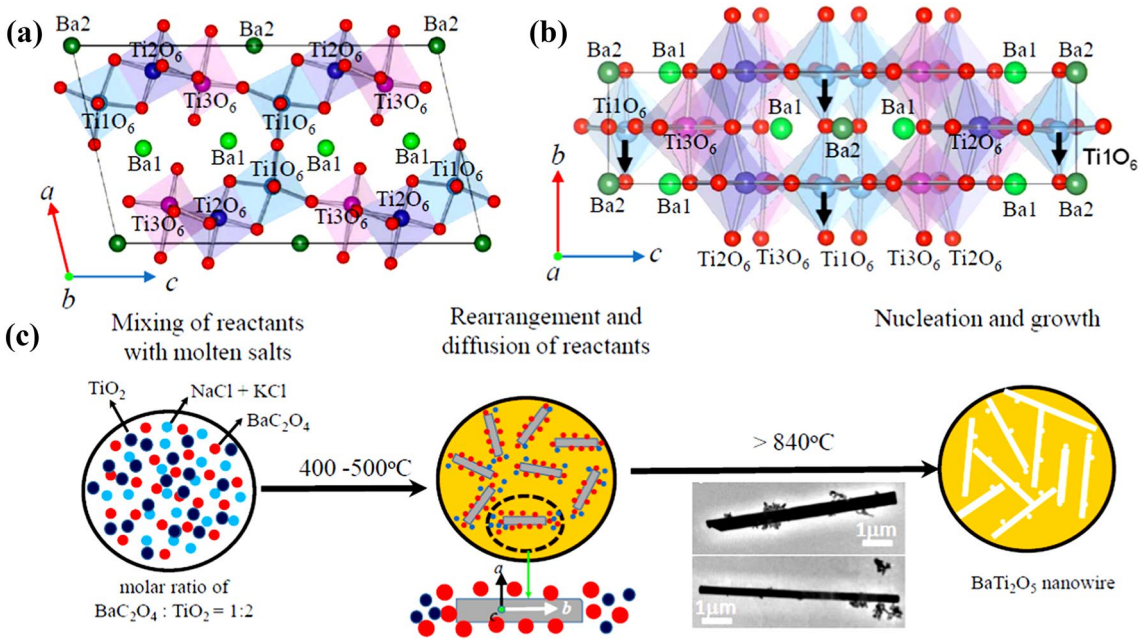

Fig. 7 Crystal structure diagrams of the BT2 with the *C*2 spacing group projected on the **a** (010) and **b** (100) planes. **c** Schematic diagram describing the formation process of BT2 nanowires in the MSS process

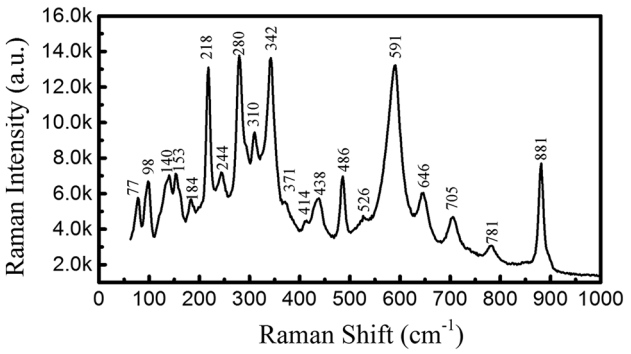

Fig. 8 Room temperature Raman spectrum of the BT2 nanowires synthesized at 900 °C (for 9 h) under the molar ratio of BaC_2O_4:TiO_2:NaCl:KCl equal to 1:2:20:20

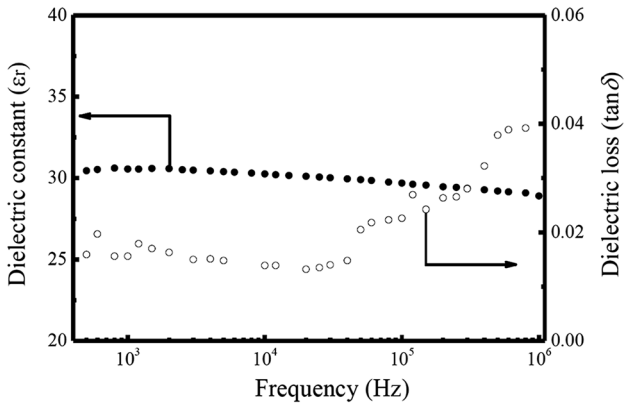

Fig. 9 Dielectric properties of the $BaTi_2O_5$ nanowires synthesized at 900 °C for 9 h by MSS method measured at room temperature with the frequency ranged from 500 to 10^6 Hz

3.4 Dielectric properties of BT2 nanowires

At room temperature the dielectric properties of BT2 nanowires synthesized at 900 °C for 9 h by MSS method were measured with the frequency ranged from 500 Hz to 1 MHz, and the results are shown in Fig. 9. A slight decrease of the dielectric constants (ε_r) of the BT2 nanowires was observed as the frequency was increased from 500 to 10^6 Hz. In the BT2 ceramics prepared from the corresponding BT2 nanowires synthesized at 900 °C for 9 h by MSS method, several types of dielectric polarizations such as space polarization, dipole orientation polarization, ionic and electronic polarizations, can make contributions to the value of the dielectric constant at low frequency, therefore, the ε_r value is high [46]. However, when the frequency is increased high enough some dielectric polarizations such as space polarization and dipole orientation polarization cannot make their contribution to the ε_r due to their failure in catching up with the reversal speed of the external electric field. Thus, the measured value of ε_r at high frequency is reduced, whereas which actually reflects the intrinsic dielectric constants of the BT2 nanowires. At 10^6 Hz, the ε_r of the BT2 nanowires was measured to be 28, and over 30 at 1 kHz. This value is very comparable

to that reported for BT2 thin films ($\varepsilon_r = 38$ at 10^6 Hz) synthesized at 900 °C prepared by sol–gel method [25]. The corresponding dielectric loss (tanδ) was kept nearly constant (about 0.01) as the frequency was increased from 500 to 30,000 Hz, and then it was increased quickly up to 0.04 at 1 MHz. This value is smaller than that reported for BT2 thin films ($\tan\delta = 0.063$ at 10^6 Hz) synthesized at 900 °C synthesized by sol–gel method [25]. It is expected that the present dielectric data will make the BT2 nanowires have great potentials in nanoscale dielectric devices.

4 Conclusions

In this work, we report on the growth of single-crystalline BT2 nanowires by MSS method. Their morphology and microstructures were investigated with focus on the influence of the MSS processing parameters (e.g., synthesized temperature, dwell time, and molten salt concentration). It is found that neither the longer dwell time nor the molten salt concentration has apparent effect on the phase structure of the BT2 nanowires, however, the synthesized temperature plays an important role in the one-dimensional morphology of the BT2 nanowires. SEM observations reveal that the one-dimensional morphology of the BT2 nanowires can be only obtained in a narrow synthesized temperature window (870–900 °C). As the synthesized temperature is as high as 970 °C, the one-dimensional morphology of BT2 nanowires is broken and they are decomposed into particles, growing into large flat crystals. The EDS results show that the BT2 nanowires are composed of Ba, Ti, and O elements with homogeneous chemical compositions, and the Ba: Ti (atomic ratio) is about 1:2.16. TEM images reveal that the BT2 nanowires synthesized at 900 °C exhibit a uniform morphology, and their average diameter is measured to be 780 nm and the average lengths is 15 μm. As the synthesized temperature is increased up to 970 °C, many BT2 nanowires are broken and decomposed into particles, growing into large flat crystals. The morphology of the BT2 nanowires with a metastable structure can be only obtained in a limited temperature window. Dielectric measurements demonstrate that the dielectric constants of BT2 nanowires synthesized at 900 °C for 9 h by MSS method are in the range of 28–31 as the frequency is ranged from 500 to 10^6 Hz. That indicates the dielectric behavior of the BT2 nanowires is almost frequency independent. The corresponding dielectric losses are generally stable (about 0.01) as the frequency is below 30,000 Hz, and then increase up to 0.04 at 10^6 Hz. Such low dielectric loss and relatively high dielectric constant promote the BT2 nanowires to be more attractive for nanoscale dielectric ceramic capacitors and resonators.

Acknowledgements The authors acknowledge the financial supports from the National Natural Science Foundation of China (Grant No. 11674161), Natural Science Foundation of Jiangsu Province (Grant No. BK20181250), higher education reform research project (Grant No. 2017JSJG086) from Jiangsu Province, as well as undergraduate teaching reform project (Grant No. 201612B5) from Nanjing University. Mr. H. Wu also would like to thank the research program B for outstanding PhD candidate (Grant No. 201802B022) from Nanjing University.

Authors' contributions XW and KL carried out the experimental works, ZP, WX, HW, and YL helped in experimental design and data analysis. ZX designed the experiments and modified the manuscript. All authors read and approved the final manuscript.

Compliance with ethical standards

Conflict of interest The authors declare that they have no conflict of interest.

References

1. Akashi T, Iwata H, Goto T (2003) Preparation of $BaTi_2O_5$ single crystal by a floating zone method. Mater Trans 44:802–804
2. Akashi T, Iwata H, Goto T (2003) Dielectric property of single crystalline $BaTi_2O_5$ prepared by a floating zone method. Mater Trans 44:1644–1646
3. Akishige Y, Fukano K, Shigematsu H (2003) New ferroelectric $BaTi_2O_5$. Jpn J Appl Phys 42:L946–L948
4. Kimura T, Goto T, Yamane H, Iwata H, Kajiwara T, Akashi T (2003) A ferroelectric barium titanate $BaTi_2O_5$. Acta Crystallogr C 59:1128–1130
5. Akishige Y, Fukano K, Shigematsu H (2004) Crystal growth and dielectric properties of new ferroelectric barium titanate: $BaTi_2O_5$. J Electroceram 13:561–565
6. Waghmare U, Sluiter MHF, Kimura T, Goto T, Kawazoe Y (2004) A lead-free high-Tc ferroelectric $BaTi_2O_5$: a first-principles study. Appl Phys Lett 84:4917–4919
7. Yashima M, Tu R, Goto T, Yamane H (2005) Crystal structure of the high-temperature paraelectric phase in barium titanate $BaTi_2O_5$. Appl Phys Lett 87:101909
8. Hushur A, Shigematsu H, Akishige Y, Kojima S (2005) Order-disorder nature of ferroelectric $BaTi_2O_5$. Appl Phys Lett 86:112903
9. Tsukada S, Fujii Y, Yoneda Y, Moriwake H, Konishi A, Akishige Y (2018) Raman scattering study of the ferroelectric phase transition in $BaTi_2O_5$. Phys Rev B 97:024116
10. Garcia V, Bibes M (2012) Inside story of ferroelectric memories. Nature 483:279–281
11. Rϕvik PM, Grande T, Einarsrud MA (2011) One-dimensional nanostructures of ferroelectric perovskites. Adv Mater 23:4007–4034
12. Zhu XH, Liu ZG, Ming NB (2010) Perovskite oxide nanotubes: synthesis, structural characterization, properties and applications. J Mater Chem 20:4015–4030
13. Zhu XH, Liu ZG, Ming NB (2010) Perovskite oxide nanowires: synthesis, property and structural characterization. J Nanosci Nanotechnol 10:4109–4123
14. Beltrain H, Gomez B, Maso N, Cordoncillo E, Escribano P, West AR (2005) Electrical properties of ferroelectric $BaTi_2O_5$ and dielectric $Ba_6Ti_{17}O_{40}$ ceramics. J Appl Phys 97:084104
15. Beltrain H, Maso N, Cordoncillo E, West AR (2007) Nanocomposite ceramics based on La-doped $BaTi_2O_5$ and $BaTiO_3$ with high temperature-independent permittivity and low dielectric loss. J Electroceram 18:277–282

16. Xu J, Akishige Y (2008) Relaxor in KF-doped $BaTi_2O_5$ ceramics by spark plasma sintering. Appl Phys Lett 92:052902
17. Akishige Y, Xu J, Shigematsu H, Morito S, Ohba T (2009) Synthesis of $BaTi_2O_5$ nanopowders by sol–gel method and the dielectric properties of the ceramics. Jpn J Appl Phys 48:051402
18. Akishige Y, Honda K, Tsukada S (2011) Synthesis and dielectric properties of Mn-doped $BaTi_2O_5$ ceramics. Jpn J Appl Phys 50:09NC10
19. Li JQ, Ba GQ, Qi XW, Li XY, Song YC, Li B (2016) Nanocrystalline $BaTi_2O_5$ dielectric ceramic prepared by full crystallization from containerless solidified glass. J Adv Ceram 5:77–83
20. Tangjuank S, Tunkasiri T (2005) Sol–gel synthesis and characterization of $BaTi_2O_5$ powders. Appl Phys A 81:1105–1107
21. Wang LQ, Kang HM, Xue DF, Liu CH (2009) Synthesis of $BaTi_2O_5$ powders by stearic acid gel method. J Cryst Growth 311:608–6010
22. Wang CB, Tu R, Goto T (2007) Ferroelectric $BaTi_2O_5$ thin film prepared by laser ablation. J Vac Sci Technol A 25:304–307
23. Wang C, Tu R, Goto T, Shen Q, Zhang L (2009) Structural and optical properties of $BaTi_2O_5$ thin films prepared by pulsed laser deposition at different substrate temperatures. Mater Chem Phys 113:130–134
24. Wang JJ, Wang CB, Shen Q, Zhang LM (2012) Preparation of ferroelectric $BaTi_2O_5$ thin films on Pt(111)/Ti/SiO_2/Si substrates by pulsed laser deposition. J Alloys Compd 512:140–143
25. Guo DY, Gong YP, Wang CB, Shen QA, Zhang L (2013) Dielectric and ferroelectric properties of $BaTi_2O_5$ thin films prepared by sol-gel method. Mater Lett 95:55–58
26. Wang L, Li GC, Zhang ZK (2006) Synthesis of $BaTi_2O_5$ nanobelts. Mate Res Bull 41:842–846
27. Yu JY, Tang SL, Wang RL, Shi YG, Nie B, Zhai L, Zhang XK, Du YW (2008) Synthesis of single-crystalline barium dititanate nanobelts. Cryst Growth Des 8:1481–1483
28. Deng Z, Dai Y, Chen W, Pei XM (2010) Synthesis and characterization of single-crystalline $BaTi_2O_5$ nanowires. J Phys Chem C 114:1748–1751
29. Guo DY, Ito A, Tu R, Goto T (2012) Growth of *b*-axis-oriented $BaTi_2O_5$ nanopillars by laser chemical vapor deposition. Key Eng Mater 508:185–188
30. Fu J, Hou YD, Zheng MP, Zhu MK (2017) Topochemical build-up of $BaTiO_3$ nanorods using $BaTi_2O_5$ as the template. CrystEngComm 19:1115–1122
31. Xue PJ, Wu H, Xia WR, Pei ZP, Lu Y, Zhu XH (2019) Molten salt synthesis of $BaTiO_3$ nanorods: dielectric, optical properties, and structural characterizations. J Am Ceram Soc 102:2325–2336
32. Fu J, Hou YD, Zheng MP, Zhu MK (2018) Regulation of the Ba/Sr Ratio of (Ba, Sr)TiO_3 and nanorod build-up through a topochemical synthesis method using $BaTi_2O_5$ as the template. Eur J Inorg Chem 26:3088–3094
33. Kimura T (2011) Advances in ceramics—synthesis and characterization. In: Sikalidis C (ed) Processing and Specific Applications. INTECH Open Access Publisher, Rijeka, p 75
34. Kimura T, Holmes MH, Newnham RE (1982) Fabrication of grain-oriented Bi_2WO_6 ceramics. J Am Ceram Soc 65:223–226
35. Li BR, Shang W, Hu ZL, Zhang NQ (2014) Template-free fabrication of pure single-crystalline $BaTiO_3$ nano-wires by molten salt synthesis technique. Ceram Int 40:73–80
36. Wu PJ, LU Y, Zhu XH (2018) Recent progress in molten salt synthesis of low-dimensional perovskite oxide nanostructures, structural characterization, properties, and functional applications: a review. J Mater Sci Technol 34:914–930
37. Yoon KH, Cho YS, Kang DH (1998) Molten salt synthesis of lead-based relaxors. J Mater Sci 33:2977–2984
38. Boltersdorf J, King N, Maggard PA (2015) Flux-mediated crystal growth of metal oxides: synthetic tunability of particle morphologies, sizes, and surface features for photocatalysis research. CrystEngComm 17:2225–2434
39. Xue PJ, Hu Y, Xia WR, Wu H, Zhu XH (2017) Molten-salt synthesis of $BaTiO_3$ powders and their atomic-scale structural characterization. J Alloys Compd 695:2870–2877
40. Vradman L, Friedland E, Zana J, Vidruk-Nehemya R, Herskowitz M (2017) Molten salt synthesis of $LaCoO_3$ perovskite. J Mater Sci 52:11383–11390
41. Leng HB (2012) Synthesis and characterization of ferroelectric $BaTi_2O_5$ nanoparticles and grain oriented ceramics. MS. D. Thesis, Wuhan Institute of Technology, Wuhan, China
42. Zhu N, West AR (2010) Formation and stability of ferroelectric $BaTi_2O_5$. J Am Ceram Soc 93:295–300
43. Chen F, Sorensen OT, Meng G, Peng D (1998) Thermal decomposition of $BaC_2O_4{\cdot}0.5H_2O$ studied by stepwise isothermal analysis and non-isothermal thermogravimetry. J Therm Anal 53:397–410
44. Voorhees PW (1992) Ostwald ripening of two-phase mixtures. Annu Rev Mater Sci 22:197–215
45. Hushur A, Kojima S, Shigematsu H, Akishige Y (2005) Raman scattering study on new ferroelectric $BaTi_2O_5$ single crystals. J Korean Phys Soc 46:86–89
46. Guo D, Wang C, Shen Q, Zhang L, Li M, Liu J (2009) Effect of measuring factors on ferroelectric properties of $Bi_{3.15}Nd_{0.85}Ti_3O_{12}$ thin films prepared by sol–gel method for non-volatile memory. Appl Phys A 97:877–881